

The effect of N-heterocyclic carbene units on the absorption spectra of Fe(II) complexes: a challenge for theory †

Olga S. Bokareva,^{*a,b} Omar Baig,^c Mohammed J. Al-Marri,^{a,d} Oliver Kühn,^a and Leticia González^c

The absorption spectra of five Fe(II) homoleptic and heteroleptic complexes containing strong sigma-donating N-heterocyclic carbene (NHC) and polypyridyl ligands have been theoretically characterized using a tuned range-separation functional. From a benchmark comparison of the obtained results against other functionals and a multiconfigurational reference, it is concluded that none of the methods is completely satisfactory to describe the absorption spectra. Using a compromised choice of 20% exact exchange, the electronic excited states underlying the absorption spectra are analyzed. The low-lying energy band of all the compounds shows predominant metal-to-ligand charge transfer (MLCT) character while the triplet excited states have metal-centered (MC) nature, which becomes more pronounced with increasing the number of NHC-donor groups. Excited MC states with partial charge transfer to the NHC-donor groups are higher in energy than comparable states without these contributions. The presence of the low-lying MC states prevents the formation of long-lived MLCT states.

1 Introduction

Transition metal organometallic complexes continue attracting attention for various catalytic applications,^{1–3} including converting and storing solar energy in a more sustainable form. The latter endeavour is highly fueled by the increasing growth of energy demands of human society and the lack of exhaustible resources. Successful examples of catalytic homogeneous and heterogeneous systems utilize noble-metal containing photosensitizers, see e.g. Refs. 4,5. However, from the economical and ecological points of view, the replacement of noble metals with earth-abundant, inexpensive, and not-toxic metal is enticing. Iron is a good candidate for this purpose. Thus, iron complexes are heavily in the spotlight, not only as promising photocatalysts, but also as convenient alternatives for conventional processing and magnetic storage of information due to their capabilities for photoinduced ultrafast spin-flip.^{6,7}

The development of new photonic materials requires understanding of the underlying photophysical processes⁹ as well as how chemical substitution influences targeted properties, such as the lifetime of charge-transfer (CT) states, the energetic ordering of the electronic excited states and the reaction yields of competing photophysical channels. In applications involving spin-flip, the interplay between local metal centered (MC) and metal-to-ligand charge-transfer (MLCT) states is also of primary importance. To this end, theoretical modeling has emerged as a powerful tool to guide and complement experimental techniques.

Due to the size of most transition metal complexes and their large number of accessible electronic excited states density func-

tional theory (DFT) and its time-dependent (TD) extension in the linear-response formulation have positioned themselves as one of the most popular computational avenues to deal with such systems, see e.g. Refs. 10–18. The capabilities of DFT to obtain ground state properties for large systems are well established,^{19,20} although results might strongly depend on the employed exchange-correlation functional.²¹ Also the deficiencies of DFT and TDDFT are well-known. The erroneous description of long-range CT properties such as ionization potentials (IP), electronic polarisabilities, and energies of CT electronic states with conventional DFT stem from the approximate description of the exchange potential, leading to a self-interaction error and wrong decay of the electron density in the long-range limit.^{22,23} Additionally, the so-called derivative discontinuity condition²⁴ is not exactly fulfilled in DFT, leading to different approaches, such as, e.g., scaled hybrids^{25,26} and range-separated hybrid functionals.^{27,28} In particular, optimally-tuned functionals have been successfully applied in a number of systems, yielding improved descriptions of various molecular properties related to fundamental and optical gaps such as IPs,^{29,30} CT and Rydberg transition energies,^{31–34} optical rotation, hyperfine couplings, and others.^{35–41}

The aim of this paper is to investigate the performance of various density functionals including tuned range-separated ones vs. a multiconfigurational reference⁴² applied to the excited-state properties of a series of iron(II) homoleptic and heteroleptic complexes that were recently synthesized by Zimmer and coworkers⁸ (see Fig. 1). These authors showed that the introduction of strong sigma-donating N-heterocyclic carbene (NHC) ligands in metal-organic complexes prompts to increase the photochemically relevant MLCT state lifetime by destabilizing e_g^* orbital energies. Here, we analyze the energetics and the nature of the electronic transitions, paying attention to the order of MLCT versus MC states, upon introducing different changes in the ligand substituents.

The rest of the manuscript is organized as follows. After a brief introduction in the theory of long-range separated functionals as well as details of multiconfigurational calculations, we present

^a Institut für Physik, Universität Rostock, Universitätsplatz 3, D-18055 Rostock, Germany. E-mail: olga.bokareva@uni-rostock.de

^b Department of Physical Chemistry, Kazan Federal University, Kremlevskaya Str. 18, 420008 Kazan, Russia

^c Institut für Theoretische Chemie, Fakultät für Chemie, Universität Wien, Währinger Str. 17 A-1090 Wien, Austria.

^d Chemical Engineering, College of Engineering, Qatar University, P.O. Box 2713, Doha, Qatar.

† Electronic Supplementary Information (ESI) available: Cartesian coordinates of all the structures and full list of electronic excited states. See DOI: 00.0000/00000000.

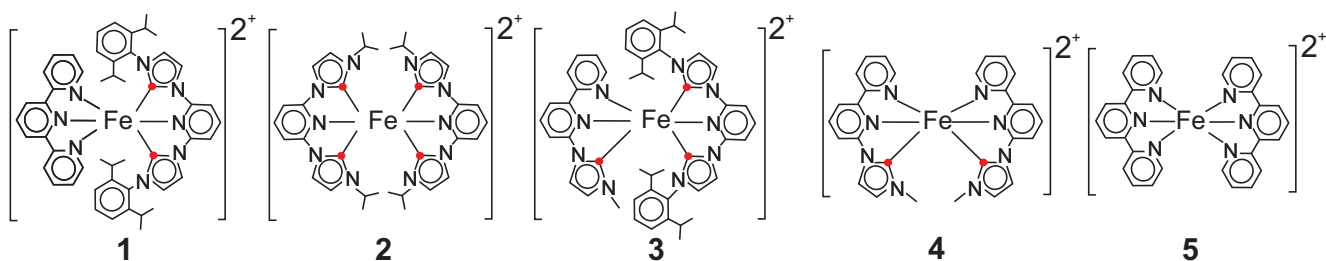


Fig. 1 Scheme of Fe(II) organometallic complexes from Ref. 8 studied in this work. Red dot indicates the NHC position.

our results on the lowest excited states and absorption spectra computed with different methods for the series of iron catalysts. We then proceed to describe the excited-state properties of the considered complexes and analyse the nature of the lowest-lying excited states, to conclude with the main findings.

2 Computational Details

The DFT functional optimization has been performed using two parameters, α and ω , for the generalized form of the short-/long-range partitioning of the Coulomb interaction⁴³ and an error function kernel $\Gamma(\omega r_{12}) = \text{erf}(\omega r_{12})$ within the LC-BLYP functional, i.e.^{44–46}

$$\frac{1}{r_{12}} = \frac{1 - [\alpha + \beta \cdot \Gamma(\omega r_{12})]}{r_{12}} + \frac{\alpha + \beta \cdot \Gamma(\omega r_{12})}{r_{12}}. \quad (1)$$

In order to tune the functional for the systems **1** to **5**, the so-called Δ SCF method^{31,47,48} has been applied. Here, the IP and EA are calculated as the differences between the ground state energies of systems with N and $N \pm 1$ electrons, i.e.

$$\text{IP}^{\alpha,\omega}(N) = E^{\alpha,\omega}(N-1) - E^{\alpha,\omega}(N), \quad (2)$$

$$\text{EA}^{\alpha,\omega}(N+1) = E^{\alpha,\omega}(N) - E^{\alpha,\omega}(N+1). \quad (3)$$

This yields separate tuning functions

$$J_0(\alpha, \omega) = |\varepsilon_{\text{HOMO}}^{\alpha,\omega}(N) + \text{IP}^{\alpha,\omega}(N)| \quad (4)$$

and

$$J_1(\alpha, \omega) = |\varepsilon_{\text{HOMO}}^{\alpha,\omega}(N+1) + \text{EA}^{\alpha,\omega}(N)|. \quad (5)$$

In order to obtain a proper description of the fundamental gap, $J_0(\alpha, \omega)$ and $J_1(\alpha, \omega)$ for IP and EA should be minimized simultaneously leading to following tuning function:^{38,49}

$$J^*(\alpha, \omega) = \sqrt{J_0^2(\alpha, \omega) + J_1^2(\alpha, \omega)}. \quad (6)$$

In principle, this function provides a manifold of (α, ω) -pairs where J^* is minimal. Selecting optimal values from those pairs requires an additional criterion. For the exact exchange-correlation density functional, the energy $E(N)$ must vary linearly for fractional electron numbers between integer N s.⁵⁰ This, however, does not hold true for many functionals. Accordingly, segments of $E(N)$ have a certain curvature (could be both positive or negative) referred to as (de)localization error,⁵¹ for a detailed discus-

sion see Ref. 41. Tuned range-separated hybrid functionals usually result in small $E(N)$ curvatures ensuring small delocalization error. However, to assist an unambiguous choice of optimal parameters, we have used the curvatures of the $E(N)$ -dependence for fractional charges and have chosen, whenever possible, the (α, ω) -pair whose curvature is closest to zero. As a particular measure of the curvature we have chosen

$$\Delta = \int_{N-1}^N dn \Delta(n) = \int_{N-1}^N dn |E(n) - E(N) - [E(N) - E(N-1)](N-n)| \quad (7)$$

to indicate the deviation from the idealized linear dependence, see also Fig. 3b.

All functional tuning calculations have been performed using the 6-31G(d) basis set for all atoms. The initial geometries have been optimized using the LC-BLYP functional with $\omega=0.17$ bohr⁻¹ which is typical for the complexes of this size.³² We note that the optimized LC-BLYP geometries are nevertheless very similar (averaged RMSD for all five complexes is 0.21, see Cartesian Coordinates in the Supporting Information[†]) to the geometries optimised with the TPSSH^{52,53} functional employed in Ref. 8. As the inclusion of an implicit solvent in this tuning procedure has been shown to deliver erroneous results,^{32,54} the optimal tuning process has been done in vacuum. The step size for varying α has been 0.05 and for ω 0.01 bohr⁻¹.

In order to calculate the final electronic excited state energies and wavefunctions, the geometries of all investigated complexes have been reoptimized employing the chosen tuned LC-BLYP functionals with corresponding α and ω values and the larger basis set def2-TZVP.⁵⁵ On these geometries, TDDFT computations were carried out with the optimally tuned LC-BLYP functional. Comparison with multiconfigurational reference data (see below) suggested an adjustment of the obtained (α, ω) -pairs.

A total of 50 singlet and 50 triplet TDDFT excited states have been calculated, expecting that this number of states is enough to capture the lowest energy region of the spectrum adequately. Solvent effects (acetonitrile) are included implicitly within the polarized continuum model approach.⁵⁶ In order to artificially add broadening to the spectra, each of the excitations have been convoluted with a Gaussian function (for the FWHM see Figure 4).

All tuning calculations were done with the Q-Chem 5.1 package⁵⁷ whereas further geometry optimizations and absorption

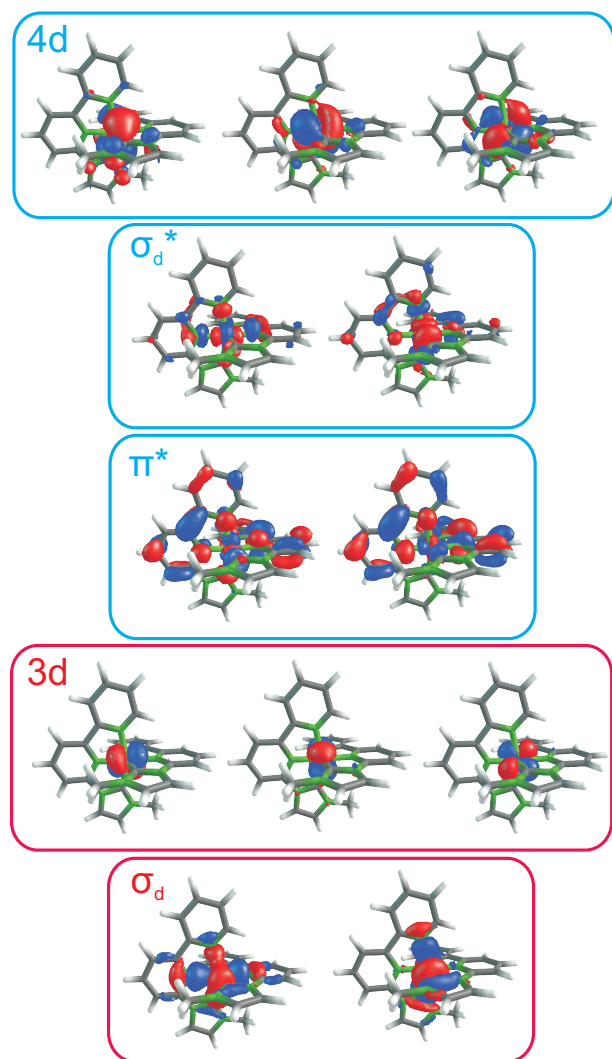


Fig. 2 Active space composition for CASSCF/CASPT2 calculations, shown on the example of complex **4**.

spectra computations were done with Gaussian 16.⁵⁸ Excited state analysis has been done using with the TheoDORE package,⁵⁹ which enables automatic quantitative wavefunction analysis and straightforward assignment of excitation localization at predefined molecular moieties.⁶⁰

For the two smallest complexes of Fig. 1 (**4** and **5**), complete active space self-consistent-field⁶¹ (CASSCF) and CAS second order perturbation theory^{62,63} (CASPT2) calculations with relativistic ANO-RCC-VTZP⁶⁴ basis set have performed as a reference using OpenMolcas.⁶⁵ The highest possible Abelian point symmetry group (C_2 for **4** and D_2 for **5**) and Cholesky decomposition have been utilized. To account for both MCLT and MC states, the active space comprised 10 electrons in the following 12 orbitals (10e/12MO): three essentially non-bonding $3d$ -orbitals of the iron atom as well three corresponding Rydbergs-like $4d$ orbitals to account for the double-shell effect, two σ_d -bonding and two σ_d^* -antibonding orbitals, and the two vacant π^* -orbitals of ligands (see Fig. 2). State-averaging with equal weights have been done over the 10 lowest states of a given symmetry and

multiplicity in CASSCF calculations; selected states have been computed with state-specific CASPT2. The frozen-core approximation have been utilized at the CASPT2 level. A default IPEA shift^{66,67} of 0.25 a.u. and an additional imaginary shift of 0.2 a.u. to cope with intruder states problem have been applied. To avoid the comparison of different solvent models in different quantum-chemistry packages, the calculations of the lowest transitions in CASPT2 and various DFT flavors (using def2-TZVP basis set) have been done in vacuum.

Depending on where electrons and holes are localized within an electronic excitation, transition metal complexes can exhibit MC, MLCT, LC, ligand-to-metal charge transfer (LMCT) or ligand-to-ligand charge transfer (LLCT) states. The nature of these states can be assigned by inspecting the orbitals involved in the electronic transition. However, this process is not only subjective but very tedious if many wave function configurations contribute to a single electronic state and on top if many electronic states are to be analysed. In this work, the assignment of the character of the states has been done using charge transfers numbers between groups of atoms defined as fragments.⁶⁰ Chemical intuition can be used to partition the molecule, but it is also possible to do a correlation analysis with subsequent hierarchical clustering⁶⁰ in order to get a comprehensive understanding of the effect a particular moiety has within a ligand. In such a procedure, charge transfer numbers are first obtained considering every atom as an independent fragment (with the exception of hydrogens that are added to the connected carbon atom and thus treated as one fragment) and then a correlation matrix of the fragments' contribution to the excited states is calculated. Through hierarchical clustering, fragments with high correlation are then combined to obtain an automatic fragmentation of each molecule. In this automatic fragmentation the threshold of the coefficient of determination R^2 can be varied, depending on the graining desired. To ease of analysis the amount of fragments should not be very high, but small enough to make chemical sense.

3 Results and Discussion

3.1 Optimization of the Range-Separation Parameters

The optimal values obtained for the range-separation parameters α and ω of the Fe(II) complexes shown in Fig. 1 are collected in Table 1. A typical example of a 2D plot of $J^*(\alpha, \omega)$ resulted from single-point calculations on the grid is presented in Fig. 3a for the complex **1**. Only for **3**, no minima have been found for the 1D curves constructed at the constant α values. In this case, we have chosen the minimal point on the $J_0(\alpha, \omega)$ 2D surface that correspond to the IP-only tuning. Importantly, the criterion of smallest piecewise curvature does not in general provide a tool to unambiguously select the best (α, ω) -pair, as this curvature is very small for such tuned functionals. An example is given in Fig. 3b for the complex **1**, where the curvatures for all (α, ω) -pairs are being two orders of magnitude smaller than for standard density functionals.⁵⁰ Based on this criterion, no exact exchange in the short-range should be included in the functional ($\alpha = 0$) for all five Fe(II) complexes (Table 1). Previously, the fraction of the exact exchange of 0.20 has been generally recommended for non-

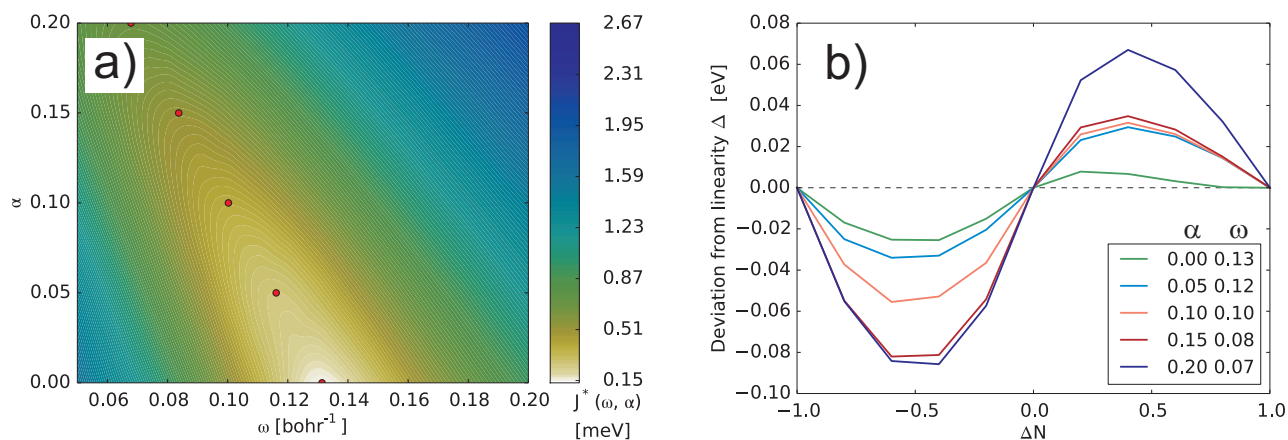


Fig. 3 a) $J^*(\alpha, \omega)$, eq. (6), for complex **1**. Red points denote minima of $J^*(\alpha, \omega)$ at constant α values. b) The deviation from linear dependence of $\Delta(n)$, see eq. (7), for complex **1**.

Table 2 Energies of lowest MLCT and MC states (singlet (S) and triplet (T), in eV) for **4** and **5** complexes predicted by CASPT2 and various DFT methods.

	CASPT2	LC ($\alpha=0.0$)	LC ($\alpha=0.15$)	LC ($\alpha=0.2$)	B3LYP	BLYP	CAM-B3LYP
4 S MLCT	2.32	2.18	2.33	2.44	2.37	1.88	3.02
4 S MC	2.53	3.42	3.12	2.91	3.03	3.40	2.81
4 T MLCT	1.81	1.81	1.99	2.23	2.18	1.62	2.78
4 T MC	2.03	2.78	2.34	2.07	2.04	2.77	2.10
5 S MLCT	2.23	2.14	2.37	2.50	2.46	1.95	3.05
5 S MC	2.27	2.83	2.59	2.50	2.49	2.84	2.43
5 T MLCT	2.23	1.80	2.07	2.21	2.18	1.64	2.51
5 T MC	1.57	2.15	1.79	1.66	1.67	2.19	1.54

Table 1 Optimized range separation parameters, α and ω , for compounds shown in Fig. 1. While $\alpha = 0$ results from optimal tuning, $\alpha = 0.2$ has been chosen for the TDDFT calculations after comparison with the CASPT2 results.

Compound	ω [bohr $^{-1}$] ($\alpha = 0.0$)	ω [bohr $^{-1}$] ($\alpha = 0.2$)
1	0.13	0.07
2	0.14	0.08
3	0.10	0.06
4	0.14	0.08
5	0.14	0.07

spin-crossover compounds^{35,37,68}. In a recent publication⁶⁹, a value of α of 0.10-0.15 has been argued to be optimal for a series of iron spin-crossover compounds after analyzing the adiabatic energy difference between high- and low-spin states based on the comparison with the OPBE reference data⁷⁰ implying that the errors inherent to the OPBE functional may also influence this conclusion.

With the constant amount of global exact exchange, the values of ω for all compounds are very close to each other, what can be rationalized by the comparable size of the ligands. The inverse value of range-separation parameter ω^{-1} reflects a characteristic distance for switching between short- and long-range parts or, in other words, an effective electron screening (delocalization) length. Previously, optimal ω values were found to decrease with increasing system size and conjugation length.^{29,36,71-77} For

Ir(III) photosensitizers of comparable size, similar ω -values of 0.14–0.18 bohr $^{-1}$ have been found.³²

3.2 Energetics of the lowest-lying electronic excited states

Table 2 collects selected energies obtained with all the methods employed in this work for complexes **4** and **5**. For this comparison, only few states – the lowest of dominantly MLCT and MC character (see systematic analysis in Section 3.4) – in both singlet and triplet manifolds have been selected; note that these states are not necessarily the two energetically lowest ones. For the tuned LC-BLYP case, three different optimal pairs of parameters (α, ω) have been considered: no constant exact exchange ($\alpha=0.0$) as it was predicted by analysis of fractional charges, as well as 15 and 20 % of exchange because those parameters have been proposed in earlier publications.^{69,70} Taken CASPT2 as a reference, one can clearly see that the purely local BLYP drastically underestimates the energies of MLCT states but overestimates the MC states. Importantly, the energies of MC states predicted with the tuned LC-BLYP ($\alpha=0.0$) almost coincide with those of BLYP, supporting the underlying assumption that at short interelectron distances the local BLYP functional dominates in Eq. (1). At the same time, it is evident that the inclusion of certain portion of exact exchange in the optimally-tuned functional may have a crucial effect on the position of MC states. Indeed, if various α values in LC-BLYP are compared, one can see that the inclusion of increasing portions of exact exchange lowers

the MC energies towards the CASPT2 reference. Simultaneously, the MLCT energies agree better with the reference. The popular B3LYP functional performs comparable to the LC-BLYP ($\alpha=0.20$), as both functionals include 20% of exact exchange. The other popular long-range functional chosen, CAM-B3LYP, gives reasonable energies for MC states but overestimates the MCLT energies.

Clearly, the test set for the comparison of the lowest energies is not large enough to deduce ultimate conclusions but the same trends have been observed for the test calculations for all studied complexes with the 6-31G(d) basis set (not shown for the sake of brevity). In addition, it is fair to keep in mind the possible inaccuracies of CASPT2 connected with the moderate size of active space and incomplete account for electron correlation. As such, the comparison above should be taken with a pinch of salt.

3.3 Vertical excitation spectra

The absorption spectra for all the complexes has been calculated using the LC-BLYP functional with $\alpha = 0.20$. This α value was chosen in accordance with the above results to reasonably describe the important MC states. The corresponding ω values can be found in Table 1.

The convoluted spectra (blue line) are compared against the experiment⁸ (black line) in Fig. 4. The blue sticks indicate the most important absorbing states calculated at the equilibrium geometry, from which the convoluted spectra has been obtained. In general, all calculated spectra show decent agreement with the experiment but they are shifted to higher energies by approximately 0.5 eV. In what follows, we shall discuss this comparison with some detail. In compound **1**, the shape of the first computed band at 2.8 eV is less broad than in the experiment and the separation between this and the next band, with an onset at 3.6 eV is larger than it should; this peak is also predicted to be closer than it should to the next one at 4.0 eV. We refrain from discussing the results at higher energies, as the number of electronic excited states included are not sufficient to map the full available experimental spectrum. In terms of shape, compound **2** shows the largest disagreement. The first experimental band of the absorption spectrum, peaking at 2.75 eV followed by a smaller peak at 3.30 eV, is not well described by theory, which shows a band from 3.25 to 4.00 eV with two peaks that experimentally are much closer together. Further, the intensities are also incorrect, with the strengths of the peaks being reverse. Noticeable is also a peak from 4.25 to 4.75 eV, which is not present in the experimental spectrum. The calculated spectrum for **3** shows two separated bands from 2.40 to 4.00 eV, which are broader in the experiment and with less separation. Part of these inaccuracies are due to the fact that our spectra are simulated at the limit of using only the equilibrium geometry, while nuclear motion affects the transition energies beyond the broadening that a Gaussian convolution would suggest.^{78,79} The compound **4** shows the best agreement with the experiment. The largest discrepancy is an additional peak at 4.00 eV. This shoulder cannot be seen in the experiment. The calculated spectrum for **5** also agrees well with the experiment. The peak at 4.25 eV is closer to the first band than in the experiment, and includes a second smaller peak at 4.50 eV that

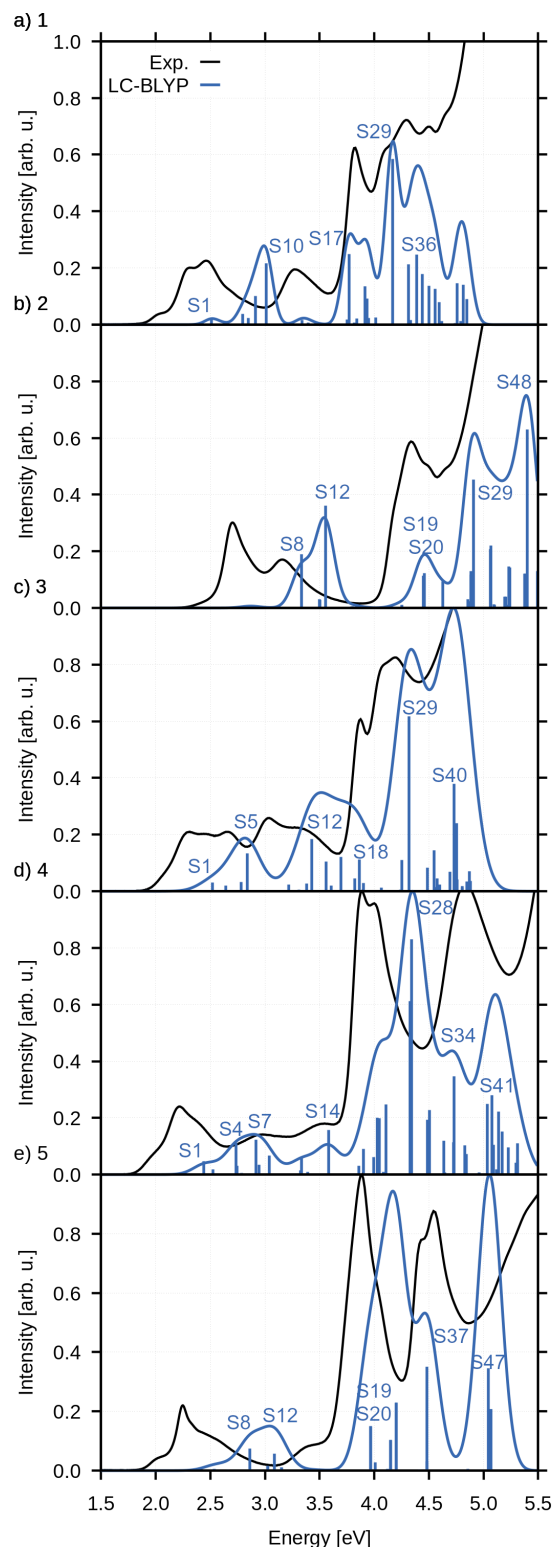


Fig. 4 Experimental⁸ and calculated absorption spectra of compounds a) **1** (FWHM 0.15 eV), b) **2** (FWHM 0.20 eV), c) **3** (FWHM 0.30 eV), d) **4** (FWHM 0.25 eV) and e) **5** (FWHM 0.25 eV) in acetonitrile. Sticks correspond to the brightest transitions calculated at the equilibrium geometry.

cannot be seen in the experiment.

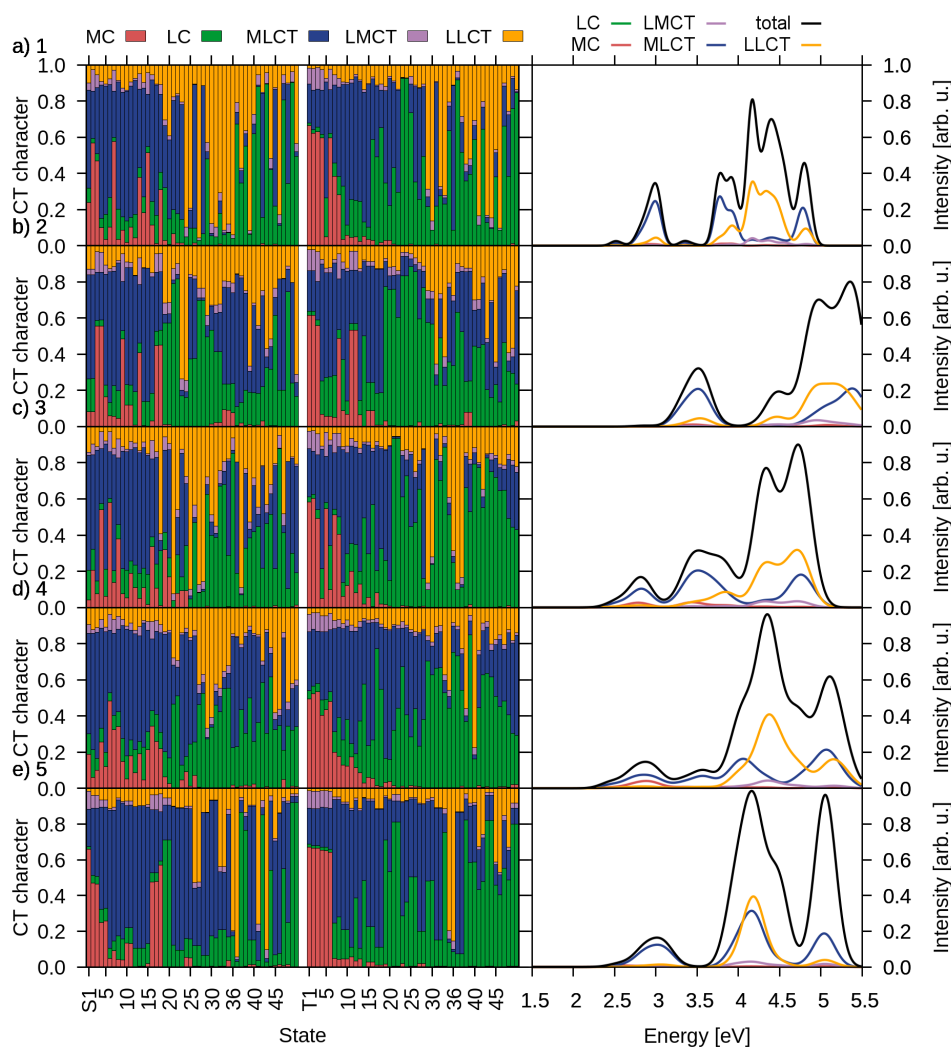


Fig. 5 Left panels: State characters of the lowest 50 singlet and 50 triplets of a) **1**, b) **2**, c) **3**, d) **4** and e) **5**. Right panels: the corresponding absorption spectra decomposed into the different contributions of the classified excited states.

3.4 Electronic state character and correlation analysis

In order to identify the electronic character of the excited states, systematic wavefunction analysis was used, where the compounds were partitioned first as the sum of three fragments: the Fe metal center and the two ligands (the polypyridyl and/or N-heterocyclic carbene (NHC) units). Fig. 5 shows the resulting assignments in each of the 50 singlet and 50 triplet states (left panels) as well as their weight to the absorption spectra (right panels) for all complexes **1-5**.

In all complexes, the lowest twenty singlet transitions are dominated by MLCT (blue boxes) and a few MC (red) excited states. For **5** these are followed by more MLCT transitions and some LC (green) and LLCT (orange) states. Interestingly, in the complexes with NHC groups **1-4** more LC and LLCT states can be seen at higher energies. If one now looks into how these states contribute to the absorption spectrum, it is clear that the low energy band is of predominant MLCT character (blue line) while the higher has contributions of both MLCT and LLCT (orange) states. The MC and LC states are mostly dark and the LMCT are in a small

amount.

Inspection of the triplet states shows a similar pattern as the singlets. The lowest triplet states have strong MC character, followed by MLCT states and then mostly LC and few LLCT states at higher energies. The lowest MC states in **5** are clustered together and have almost identical, high coefficients for the MC state. They are followed by states with almost no MC contributions. This is not true for the complexes with NHC ligands. For complexes **1** and **4**, both with two NHC donors, some differences can be appreciated. In **1** the singlet MC states are lower than in **4** but the low energy triplets of both complexes are of MC character, except for T5 in **1**. This MLCT state breaks up the series of MC states. In **3**, with 3 NHC donors, the cluster of low energy MC states is broken up by two MLCT states. Finally in the compound with 4 NHC donors, **2**, the MC states cluster even less. Instead, several MLCT states are lower in energy than half of the MC states. This behaviour is in agreement with the results of Ref. 8 where an increased number of NHC donors led to a destabilisation of the high-spin MC states. This in turn leads to increased ³MLCT

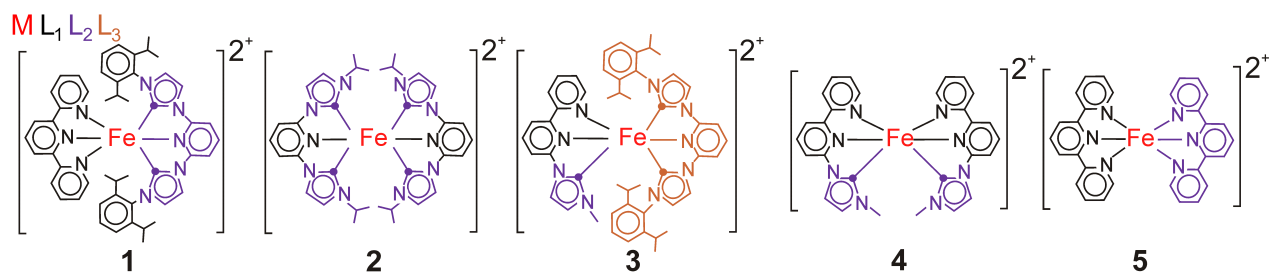


Fig. 6 Fragmentation scheme for the investigation of the role of the NHC-fragments. Atoms coloured the same way are part of the same fragment. Dots indicate NHC-donors.

lifetimes.

Albeit informative, the previous fragmentation scheme with all equivalent ligands prevents one to know which ligand in particular is involved in the excitation or whether the charge prefers a particular region within the ligand. Moreover, this particular fragmentation scheme has been enforced based on chemical intuition, but not on the actual distribution of density within the molecule. If instead a correlation analysis with subsequent hierarchical clustering is done the fragmentation depicted in Fig. 6 is obtained. With two identical polypyridyl ligands, the homoleptic complex **5** is the simplest of all the complexes and as expected, the automatic fragmentation procedure provides three fragments, the Fe center and the two ligands as separate fragments, as chemical intuition would do. Despite also being homoleptic, this is not the case for **4**. Here the automatic fragmentation separates the NHC-rings of the ligands and collects them in one fragment. The other two rings of each ligand are considered a single fragment. With the same thresholds, the results for **3** initially led to five fragments. One consisted of the 2,6-diisopropylphenyl (dipp) groups alone. However, this fragment does not play a big role in the excitations and thus has low correlation with the other fragments. Therefore, the dipp-groups were added to the fragment with their neighbouring NHC-rings. The other ligand is split into two parts, the NHC-ring and the polypyridyl rings, making the four fragments that are depicted in Fig. 6. The results and fragmentation scheme for **2** are similar to those of **4**: The NHC-rings are separated and collected into one ligand while the two central pyridyl rings form the other ligand for the analysis. The fragments obtained in **1** can be compared to those for **3**: The NHC ligands and the central pyridyl ring connecting them are collected in one fragment. The unsubstituted terpyridine ligand is collected as another fragment. In contrast to **3** the clustering favours adding the dipp groups to the terpyridine ring of the other ligand, not the neighbouring NHC groups.

In conclusion, the correlation analysis provides two important messages. The first is that the NHC groups have a clear effect in the photophysics of these complexes. The second is that this effect is different depending on how the carbenes are incorporated into the ligands –and this effect is difficult to predict a priori. Interestingly, the charge density is not necessarily fully delocalized over the whole ligand, but different NHC fragments induce localized excitations and should be considered as independent fragments.

Note that, the central iron atom is always considered as one

fragment for the analysis so that the MC, LMCT and MLCT transitions can still be identified as it is conventional in coordination chemistry. In contrast, LC and LLCT states in the following results do not correspond directly to conventional LC and LLCT states because the ligands are broken and clustered in a different way than intuition might dictate. However, it is always possible to consider their sum, reaching the same rough assignment as one would do in Fig. 5.

In the following, we will analyse the particular roles of each of these fragments by inspecting the corresponding CT numbers among them, as depicted in Fig. 7. We start with **5** because with two symmetric and identical ligands is the simplest and can be used as a reference. Its two ligands are labeled as L_1 and L_2 . As expected, the ligands contribute symmetrically to most excitations, which for simplicity are indicated by different shades of the same color. States with asymmetrical contributions can usually be found as pairs of degenerate states. These states have almost identical energies (see Table 6 in the SI[†]) and contributions, but the L_1 and L_2 terms are switched. Example pairs are S2 and S3, S4 and S5. In **4**, the polypyridyl rings are collected into L_1 and the NHC rings in L_2 . One can see that CT to the NHC rings plays a role in virtually all of the MLCT contributions, justifying this separation. In **3**, it can be seen that the single unsubstituted NHC ring in L_2 does not play a role in most of the excited states. In particular, it contributes to almost no MLCTs. The MC triplet states higher in energy show no ML_1CT or ML_2CT contributions, indicating that the dipp-substituted NHC-donors of L_3 are more important here. The four NHC rings of **2**, collected in L_2 , contribute to most MLCT transitions at least partially. In addition it can be seen that MC states with larger ML_2CT than ML_1CT contributions are higher in energy. This is similar to the results for **3**, where the substituted NHC-donors seem important for the increasing MC energies. CT from L_2 occurs in the higher energy states to the pyridyl rings of L_1 . Compound **1** has the least contributions of the fragment with NHC donors, L_2 . It can be clearly seen that the highest MC states of both the singlets and triplets have ML_2CT contributions. MLCT states characterised by contributions of L_2 are also generally higher in energy than those with charge transfer to L_1 .

The automatic fragmentation clearly identified the NHC groups as separate contributors to the excitations. Those contributions were generally larger for higher energy excitations. Both low-energy MLCT and MC states are generally higher in energy if they

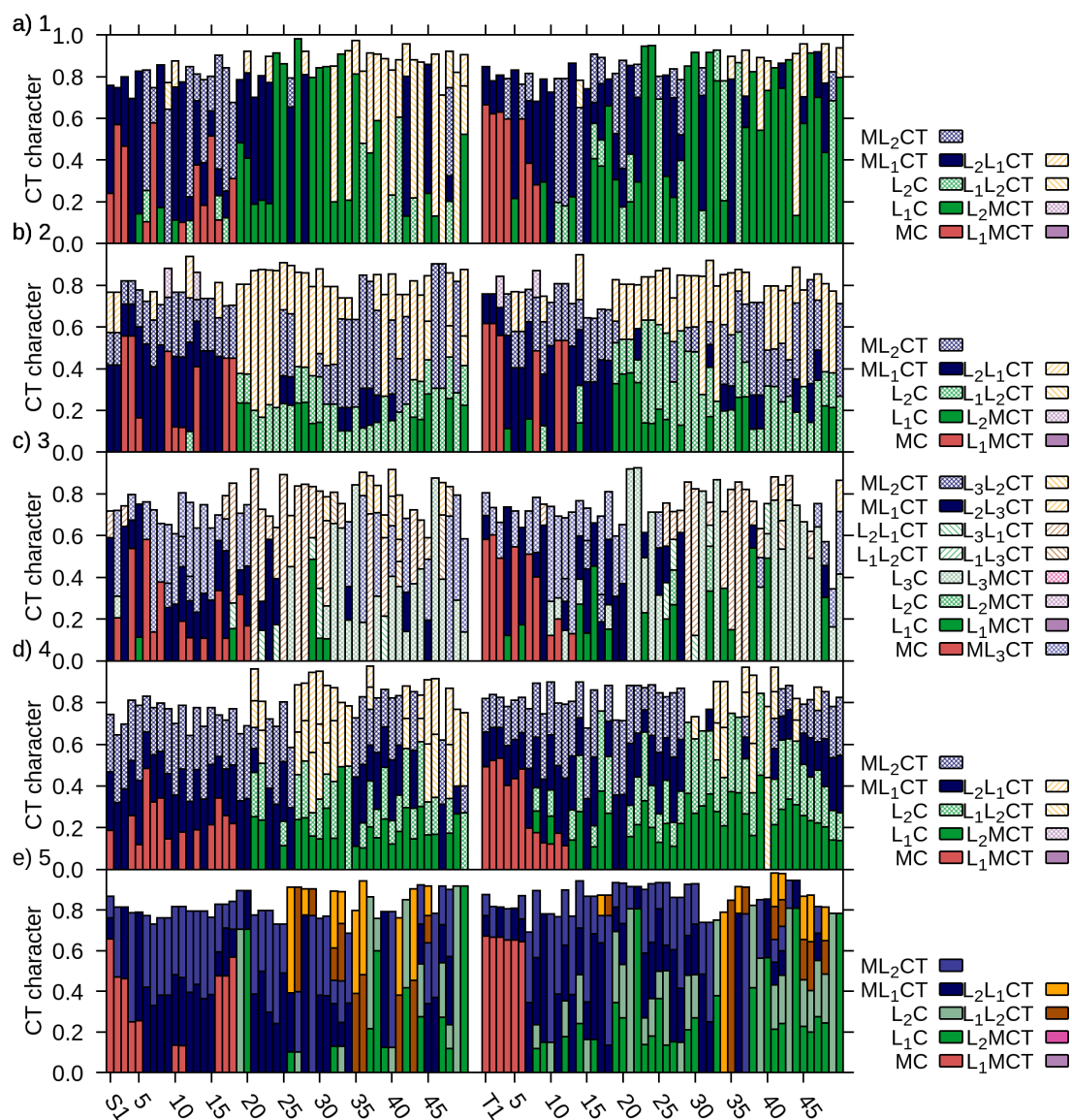


Fig. 7 State characters of the lowest 50 singlets and triplets of a) **1**, b) **2**, c) **3**, d) **4** and e) **5** using the fragmentation scheme shown in Fig. 6. The colors are toned to indicate metal-centered (MC), ligand-centered (LC), metal-to-ligand charge transfer (MLCT) and ligand-to-ligand charge transfer (LLCT) states, considering L_1 , L_2 and L_3 . Patterned bars indicate that a fragment involved contains an NHC-group. Contributions smaller than 0.1 have been omitted for ease of viewing.

include contributions of charge transfer to a NHC fragment. Nevertheless, this effect seems to be stronger for the MC states. The reference molecule with no NHC donors **5** has clustered MC states as the lowest states of both singlet and triplet excitations. In contrast, with increasing number of NHC donors more MC states are shifted higher than some MLCT states in both singlets and triplets.

4 Conclusions

In this work, we have investigated five Fe(II) homoleptic and heteroleptic complexes that include strong sigma-donating N-heterocyclic carbene and polypyridyl ligands with the aim to characterize the effect of the carbene moiety on the position of MLCT and MC excited states. For this purpose, the absorption spectra of the complexes was calculated with an optimally-tuned range

separation functional, LC-BLYP. To benchmark the LC-BLYP functional beyond the usual conditions for optimal tuning, selected low-lying singlets and triplet excited states of MLCT and MC character were computed in gas phase at different levels of theory. Methods besides the LC-BLYP functional where the influence of the α and ω tuning parameters was explored, include the BLYP, B3LYP and CAM-B3LYP functionals as well as CASPT2, which was taken as a reference. The results indicate that none of these DFT approaches are completely satisfactory for these complexes. Compared to the CASPT2 reference, the tuned LC-BLYP with a constant portion of exact exchange of 20% was taken as a compromise. This provided a reasonable description of the absorption spectra of the complexes with which the comparison was made and spectra of different quality in the rest of the com-

plexes. The discrepancies between theory and experiment point to the fact that tuning towards particular transitions (two low-lying MC and MLCT CASPT2 states) does not necessarily provide a uniform improvement across the spectrum, hinting to strong differential correlation⁸⁰ in these complexes.

The analysis of the electronic excited states underlying the absorption spectra with the chosen tuned LC-BLYP functional shows that excitation occurs to singlet states of predominant MLCT character. As expected for non-emissive iron complexes the triplet excited states have MC nature in the lowest part of the absorption spectrum, followed by MLCT states. Increasing the number of NHC-donor groups leads to a blue shift of only a part of these triplet MC states. But, some of them stay in the low-energy region thus preventing the presence of long-lived MLCT states.

Overall, this paper also highlights the usefulness of quantitative wave function analysis and hierarchical clustering, as it reveals how the carbene rings play an important individual role in the excitations, by localizing part of the electron density in the excitation. We expect that the gained insight can be useful in the design of alternative Fe(II) complexes with long-lived MLCT states.

Conflicts of interest

There are no conflicts to declare.

Acknowledgements

This work has been financially supported by the Deutsche Forschungsgemeinschaft SPP 2102 "Light Controlled Reactivity of Metal Complexes" (GO 1059/8-1 and KU 952/12-1) and by Ministry of Education and Science of Russian Federation (Grant No. 14.Y26.31.0019). The Vienna Scientific Cluster and the University of Vienna are thanked for generous allocation of computer resources.

Notes and references

- 1 A. J. Esswein and D. G. Nocera, *Chem. Rev.*, 2007, **107**, 4022–47.
- 2 M. Hamburger, G. F. Moore, D. M. Kramer, D. Gust, A. L. Moore and T. A. Moore, *Chem. Soc. Rev.*, 2009, **38**, 25–35.
- 3 R. E. Blankenship, D. M. Tiede, J. Barber, G. W. Brudvig, G. Fleming, M. Ghirardi, M. R. Gunner, W. Junge, D. M. Kramer, A. Melis, T. A. Moore, C. C. Moser, D. G. Nocera, A. J. Nozik, D. R. Ort, W. W. Parson, R. C. Prince and R. T. Sayre, *Science*, 2011, **332**, 805–9.
- 4 A. Hagfeldt, G. Boschloo, L. Sun, L. Kloo and H. Pettersson, *Chem. Rev.*, 2010, **110**, 6595–663.
- 5 W. T. Eckenhoff and R. Eisenberg, *Dalton Trans.*, 2012, **41**, 13004–21.
- 6 A. Bousseksou, G. Molnár, L. Salmon and W. Nicolazzi, *Chem. Soc. Rev.*
- 7 *Spin-Crossover Materials: Properties and Applications*, ed. M. A. Halcrow, Wiley, Chichester, West Sussex, United Kingdom, 2013.
- 8 P. Zimmer, L. Burkhardt, A. Friedrich, J. Steube, A. Neuba, R. Schepper, P. Müller, U. Flörke, M. Huber, S. Lochbrunner and M. Bauer, *Inorg. Chem.*, 2018, **57**, 360–373.
- 9 Y. You and W. Nam, *Chem. Soc. Rev.*, 2012, **41**, 7061–84.
- 10 L. L. Tinker, N. D. McDaniel, P. N. Curtin, C. K. Smith, M. J. Ireland and S. Bernhard, *Chemistry*, 2007, **13**, 8726–32.
- 11 X.-N. Li, Z.-J. Wu, H.-J. Zhang, X.-J. Liu, L. Zhou, Z.-F. Li and Z.-J. Si, *Phys. Chem. Chem. Phys.*, 2009, **11**, 6051–6059.
- 12 R. D. Costa, P. M. Viruela, H. J. Bolinka and E. Ortí, *J. Mol. Struct.*, 2009, **912**, 21–26.
- 13 N. Tian, D. Lenkeit, S. Pelz, L. H. Fischer, D. Escudero, R. Schiewek, D. Klink, O. J. Schmitz, L. González, M. Schäferling and E. Holder, *Eur. J. Inorg. Chem.*, 2010, 4875–4885.
- 14 S. Ladouceur, D. Fortin and E. Zysman-Colman, *Inorg. Chem.*, 2010, **49**, 5625–5641.
- 15 S.-H. Wu, J.-W. Ling, S.-H. Lai, M.-J. Huang, C. H. Cheng and I.-C. Chen, 2010, **114**, 10339–10344.
- 16 S.-y. Takizawa, K. Shimada, Y. Sato and S. Murata, *Inorg. Chem.*, 2014, **53**, 2983–95.
- 17 D. N. Chirdon, W. J. Transue, H. N. Kagalwala, A. Kaur, A. B. Maurer, T. Pintauer and S. Bernhard, *Inorg. Chem.*, 2014, **53**, 1487–99.
- 18 M.-X. Song, G.-F. Wang, J. Wang, Y.-H. Wang, F.-Q. Bai and Z.-K. Qin, *Spectr. Acta*, 2014, **134C**, 406–412.
- 19 S. F. Sousa, P. A. Fernandes and M. J. a. Ramos, 2007, **111**, 10439–52.
- 20 R. O. Jones, *Rev. Mod. Phys.*, 2015, **87**, 897–923.
- 21 S. I. Bokarev, O. S. Bokareva and O. Kühn, *J. Chem. Phys.*, 2012, **136**, 214305.
- 22 A. Dreuw and M. Head-Gordon, 2005, **105**, 4009–4037.
- 23 M. J. G. Peach, P. Benfield, T. Helgaker and D. J. Tozer, *J. Chem. Phys.*, 2008, **128**, 44118.
- 24 E. Kraisler and L. Kronik, *J. Chem. Phys.*, 2014, **140**, 18A540.
- 25 A. D. Becke, *J. Chem. Phys.*, 1993, **98**, 1372.
- 26 C. Adamo and V. Barone, *J. Chem. Phys.*, 1998, **108**, 664.
- 27 A. Savin, A. Savin, WORLD SCIENTIFIC, 1995, vol. 1.
- 28 T. Leininger, H. Stoll, H.-J. Werner and A. Savin, *Chem. Phys. Lett.*, 1997, **275**, 151–160.
- 29 S. Refaely-Abramson, R. Baer and L. Kronik, *Phys. Rev. B*, 2011, **84**, 075144.
- 30 M. P. Borpuzari and R. Kar, *J. Comp. Chem.*, 2017, **38**, 2258–2267.
- 31 T. Stein, L. Kronik and R. Baer, *J. Amer. Chem. Soc.*, 2009, **131**, 2818–20.
- 32 O. S. Bokareva, G. Grell, S. I. Bokarev and O. Kühn, *J. Chem. Theor. Comp.*, 2015, **11**, 1700–1709.
- 33 S. I. Bokarev, O. S. Bokareva and O. Kühn, *Coord. Chem. Rev.*, 2015, **304-305**, 133–145.
- 34 S. Fischer, O. S. Bokareva, E. Barsch, S. I. Bokarev, O. Kühn and R. Ludwig, *ChemCatChem*, 2016, **8**, 404–411.
- 35 S. Refaely-Abramson, S. Sharifzadeh, N. Govind, J. Autschbach, J. B. Neaton, R. Baer and L. Kronik, *Phys. Rev. Lett.*, 2012, **109**, 226405.
- 36 T. Körzdörfer, J. S. Sears, C. Sutton and J.-L. Brédas, *J. Chem.*

- Phys.*, 2011, **135**, 204107.
- 37 D. A. Egger, S. Weissman, S. Refaely-Abramson, S. Sharifzadeh, M. Dauth, R. Baer, S. Kümmel, J. B. Neaton, E. Zojer and L. Kronik, *J. Chem. Theor. Comp.*, 2014, **10**, 1934–1952.
- 38 A. Karolewski, L. Kronik and S. Kümmel, *J. Chem. Phys.*, 2013, **138**, 204115.
- 39 M. Srebro and J. Autschbach, *J. Chem. Theor. Comp.*, 2012, **8**, 245–256.
- 40 M. Srebro and J. Autschbach, *J. Phys. Chem. Lett.*, 2012, **3**, 576–581.
- 41 J. Autschbach and M. Srebro, *Acc. Chem. Res.*, 2014, **47**, 2592–602.
- 42 S. Mai and L. González, *Angewandte Chemie International Edition*, 2020.
- 43 T. Yanai, D. P. Tew and N. C. Handy, *Chem. Phys. Lett.*, 2004, **393**, 51–57.
- 44 H. Iikura, T. Tsuneda, T. Yanai and K. Hirao, *J. Chem. Phys.*, 2001, **115**, 3540–3544.
- 45 Y. Tawada, T. Tsuneda, S. Yanagisawa, T. Yanai and K. Hirao, *J. Chem. Phys.*, 2004, **120**, 8425–8433.
- 46 M. Chiba, T. Tsuneda and K. Hirao, *J. Chem. Phys.*, 2006, **124**, 144106.
- 47 E. Livshits and R. Baer, *Phys. Chem. Chem. Phys.*, 2007, **9**, 2932–41.
- 48 T. Stein, L. Kronik and R. Baer, *J. Chem. Phys.*, 2009, **131**, 244119.
- 49 L. Kronik, T. Stein, S. Refaely-Abramson and R. Baer, *J. Chem. Theor. Comp.*, 2012, **8**, 1515–1531.
- 50 M. Dauth, F. Caruso, S. Kümmel and P. Rinke, *Phys. Rev. B*, 2016, **93**, year.
- 51 A. Cohen, P. Mori-Sánchez and W. Yang, *Phys. Rev. B*, 2008, **77**, 115123.
- 52 J. Tao, J. P. Perdew, V. N. Staroverov and G. E. Scuseria, *Phys. Rev. Lett.*, 2003, **91**, 146401.
- 53 V. N. Staroverov, G. E. Scuseria, J. Tao and J. P. Perdew, *J. Chem. Phys.*, 2004, **121**, 11507.
- 54 L. Kronik and S. Kümmel, *Adv. Mater.*, 2018, **30**, 1706560.
- 55 F. Weigend and R. Ahlrichs, *Phys. Chem. Chem. Phys.*, 2005, **7**, 3297–3305.
- 56 J. Tomasi, B. Mennucci and R. Cammi, *Chem. Rev.*, 2005, **105**, 2999–3093.
- 57 Y. Shao, Z. Gan, E. Epifanovsky, A. T. Gilbert, M. Wormit, J. Kussmann, A. W. Lange, A. Behn, J. Deng, X. Feng, D. Ghosh, M. Goldey, P. R. Horn, L. D. Jacobson, I. Kaliman, R. Z. Khaliullin, T. Kus, A. Landau, J. Liu, E. I. Proynov, Y. M. Rhee, R. M. Richard, M. A. Rohrdanz, R. P. Steele, E. J. Sundstrom, H. L. W. III, P. M. Zimmerman, D. Zuev, B. Albrecht, E. Alguire, B. Austin, G. J. O. Beran, Y. A. Bernard, E. Berquist, K. Brandhorst, K. B. Bravaya, S. T. Brown, D. Casanova, C.-M. Chang, Y. Chen, S. H. Chien, K. D. Closser, D. L. Crittenden, M. Diedenhofen, R. A. D. Jr., H. Do, A. D. Dutoi, R. G. Edgar, S. Fatehi, L. Fusti-Molnar, A. Ghysels, A. Golubeva-Zadorozhnaya, J. Gomes, M. W. Hanson-Heine, P. H. Harbach, A. W. Hauser, E. G. Hohenstein, Z. C. Holden, T.-C. Jagau, H. Ji, B. Kaduk, K. Khistyayev, J. Kim, J. Kim, R. A. King, P. Klunzinger, D. Kosenkov, T. Kowalczyk, C. M. Krauter, K. U. Lao, A. D. Laurent, K. V. Lawler, S. V. Levchenko, C. Y. Lin, F. Liu, E. Livshits, R. C. Lochan, A. Luenser, P. Manohar, S. F. Manzer, S.-P. Mao, N. Mardirossian, A. V. Marenich, S. A. Maurer, N. J. Mayhall, E. Neuscamman, C. M. Oana, R. Olivares-Amaya, D. P. O'Neill, J. A. Parkhill, T. M. Perrine, R. Peverati, A. Prociuk, D. R. Rehn, E. Rosta, N. J. Russ, S. M. Sharada, S. Sharma, D. W. Small, A. Sodt, T. Stein, D. Stück, Y.-C. Su, A. J. Thom, T. Tsuchimochi, V. Vanovschi, L. Vogt, O. Vydrov, T. Wang, M. A. Watson, J. Wenzel, A. White, C. F. Williams, J. Yang, S. Yeganeh, S. R. Yost, Z.-Q. You, I. Y. Zhang, X. Zhang, Y. Zhao, B. R. Brooks, G. K. Chan, D. M. Chipman, C. J. Cramer, W. A. G. III, M. S. Gordon, W. J. Hehre, A. Klamt, H. F. S. III, M. W. Schmidt, C. D. Sherrill, D. G. Truhlar, A. Warshel, X. Xu, A. Aspuru-Guzik, R. Baer, A. T. Bell, N. A. Besley, J.-D. Chai, A. Dreuw, B. D. Dunietz, T. R. Furlani, S. R. Gwaltney, C.-P. Hsu, Y. Jung, J. Kong, D. S. Lambrecht, W. Liang, C. Ochsenfeld, V. A. Rassolov, L. V. Slipchenko, J. E. Subotnik, T. V. Voorhis, J. M. Herbert, A. I. Krylov, P. M. Gill and M. Head-Gordon, *Molecular Physics*, 2015, **113**, 184–215.
- 58 M. J. Frisch, G. W. Trucks, H. B. Schlegel, G. E. Scuseria, M. A. Robb, J. R. Cheeseman, G. Scalmani, V. Barone, G. A. Petersson, H. Nakatsuji, X. Li, M. Caricato, A. V. Marenich, J. Bloino, B. G. Janesko, R. Gomperts, B. Mennucci, H. P. Hratchian, J. V. Ortiz, A. F. Izmaylov, J. L. Sonnenberg, D. Williams-Young, F. Ding, F. Lipparini, F. Egidi, J. Goings, B. Peng, A. Petrone, T. Henderson, D. Ranasinghe, V. G. Zakrzewski, J. Gao, N. Rega, G. Zheng, W. Liang, M. Hada, M. Ehara, K. Toyota, R. Fukuda, J. Hasegawa, M. Ishida, T. Nakajima, Y. Honda, O. Kitao, H. Nakai, T. Vreven, K. Throssell, J. A. Montgomery, Jr., J. E. Peralta, F. Ogliaro, M. J. Bearpark, J. J. Heyd, E. N. Brothers, K. N. Kudin, V. N. Staroverov, T. A. Keith, R. Kobayashi, J. Normand, K. Raghavachari, A. P. Rendell, J. C. Burant, S. S. Iyengar, J. Tomasi, M. Cossi, J. M. Millam, M. Klene, C. Adamo, R. Cammi, J. W. Ochterski, R. L. Martin, K. Morokuma, O. Farkas, J. B. Foresman and D. J. Fox, *Gaussian16 Revision A.03*, 2016, Gaussian Inc. Wallingford CT.
- 59 F. Plasser, *TheoDORE: A Package for Theoretical Density, Orbital Relaxation, and Exciton Analysis*, Available at <http://theodore-qc.sourceforge.net/>.
- 60 S. Mai, F. Plasser, J. Dorn, M. Fumanal, C. Daniel and L. González, *Coord. Chem. Rev.*, 2018, **361**, 74 – 97.
- 61 B. O. Roos, P. R. Taylor and P. E. Sigbahn, *Chem. Phys.*, 1980, **48**, 157–173.
- 62 K. Andersson, P.-Å. Malmqvist and B. Roos, *J. Chem. Phys.*, 1992, **96**, 1218–1226.
- 63 K. Andersson, P.-Å. Malmqvist, B. O. Roos, A. J. Sadlej and K. Wolinski, *J. Phys. Chem.*, 1990, **94**, 5483–5488.
- 64 B. O. Roos, R. Lindh, P.-Å. Malmqvist, V. Veryazov and P.-O. Widmark, *J. Phys. Chem. A*, 2004, **108**, 2851—2858.
- 65 I. Fdez. Galván, M. Vacher, A. Alavi, C. Angeli, F. Aquilante, J. Autschbach, J. J. Bao, S. I. Bokarev, N. A. Bogdanov, R. K. Carlson, L. F. Chibotaru, J. Creutzberg, N. Dattani, M. G. Del-

- cey, S. S. Dong, A. Dreuw, L. Freitag, L. M. Frutos, L. Gagliardi, F. Gendron, A. Giussani, L. González, G. Grell, M. Guo, C. E. Hoyer, M. Johansson, S. Keller, S. Knecht, G. Kovačević, E. Källman, G. Li Manni, M. Lundberg, Y. Ma, S. Mai, J. P. Malhado, P.-Å. Malmqvist, P. Marquetand, S. A. Mewes, J. Norell, M. Olivucci, M. Oppel, Q. M. Phung, K. Pierloot, F. Plasser, M. Reiher, A. M. Sand, I. Schapiro, P. Sharma, C. J. Stein, L. K. Sørensen, D. G. Truhlar, M. Ugandi, L. Ungur, A. Valentini, S. Vancoillie, V. Veryazov, O. Weser, T. A. Wesolowski, P.-O. Widmark, S. Wouters, A. Zech, J. P. Zobel and R. Lindh, *J. Chem. Theor. Comp.*, 2019, **15**, 5925–5964.
- 66 G. Ghigo, B. O. Roos and P.-Å. Malmqvist, *Chem. Phys. Lett.*, 2004, **396**, 142–149.
- 67 J. P. Zobel, J. J. Nogueira and L. González, *Chem. Sci.*, 2017, **8**, 1482–1499.
- 68 M. A. Rohrdanz, K. M. Martins and J. M. Herbert, *J. Chem. Phys.*, 2009, **130**, 054112.
- 69 G. Prokopiou and L. Kronik, *Chemistry - A European Journal*, 2018, **24**, 5173–5182.
- 70 M. Swart, *J. Chem. Theor. Comp.*, 2008, **4**, 2057–2066.
- 71 T. Stein, H. Eisenberg, L. Kronik and R. Baer, *Phys. Rev. Lett.*, 2010, **105**, 266802.
- 72 A. Karolewski, T. Stein, R. Baer and S. Kümmel, *J. Chem. Phys.*, 2011, **134**, 151101.
- 73 M. J. G. Peach and D. J. Tozer, *J. Phys. Chem. A*, 2012, **116**, 9783–9789.
- 74 M. Casida and M. Huix-Rotllant, *Annu. Rev. Phys. Chem.*, 2012, **63**, 287–323.
- 75 M. J. G. Peach, M. J. Williamson and D. J. Tozer, *J. Chem. Theor. Comp.*, 2011, **7**, 3578–3585.
- 76 J. S. Sears, T. Koerzdoerfer, C.-R. Zhang and J.-L. Brédas, *J. Chem. Phys.*, 2011, **135**, 151103.
- 77 U. Salzner and A. Aydin, *J. Chem. Theor. Comp.*, 2011, 2568–2583.
- 78 J. J. Nogueira and L. González, *Annu. Rev. Phys. Chem.*, 2018, **69**, 473–497.
- 79 S. Bai, R. Mansour, L. Stojanović, J. M. Toldo and M. Barbatti, *J. Mol. Model.*, 2020, **26**, 107.
- 80 L. González, D. Escudero and L. Serrano-Andrés, *ChemPhysChem*, 2012, **13**, 28–51.